Decadal–Multidecadal Variations of Asian Summer Rainfall from the Little Ice Age to the Present

HUI SHI

Department of Atmospheric Sciences, School of Ocean and Earth Science and Technology, University of Hawai'i at Mānoa, Honolulu, Hawaii

BIN WANG

Department of Atmospheric Sciences, School of Ocean and Earth Science and Technology, University of Hawai'i at Mānoa, Honolulu, Hawaii, and Earth System Modeling Center, Nanjing University of Information Science and Technology, Nanjing, China

JIAN LIU

Key Laboratory of Virtual Geographic Environment of Ministry of Education, School of Geography Science, Nanjing Normal University, Nanjing, China

FEI LIU

Earth System Modeling Center, Nanjing University of Information Science and Technology, Nanjing, China

(Manuscript received 31 October 2018, in final form 5 August 2019)

ABSTRACT

Features of decadal–multidecadal variations of the Asian summer rainfall are revealed by analysis of the reconstructed Asian summer precipitation (RAP) dataset from 1470 to 2013. Significant low-frequency periodicities of the all-Asian rainfall (AAR) index (AARI) are found on decadal (8–10 yr), quasi-bidecadal (22 yr), and multidecadal (50–54 yr) time scales, as well as centennial time scales. The decadal and multidecadal peaks are mainly from the "monsoon Asia" area and the Maritime Continent, while the 22-yr peak is from the "arid Asia" area. A remarkable change of leading frequency from multidecadal to decadal after AD 1700 is detected across the entire Asian landmass. The leading empirical orthogonal function (EOF) modes on the decadal and multidecadal time scales exhibit a uniform structure similar to that on the interannual time scale, suggesting a cross-time-scale, in-phase variation of the rainfall across continental Asia and the Maritime Continent. Enhanced AAR on a decadal time scale is found associated with the mega-La Niña sea surface temperature (SST) pattern over the Pacific. The AARI–mega-ENSO (El Niño–Southern Oscillation) relationship is persistently significant except from 1820 to around 1900. Enhanced decadal AAR is also found to be associated with extratropical North Atlantic warming. The AARI–AMO (Atlantic multidecadal oscillation) relationship, however, is nonstationary. On the multidecadal time scale, the AAR is significantly related to the AMO. Mechanisms associated with the decadal–multidecadal variability of AAR are also discussed.

1. Introduction

The Asian monsoon and global monsoon vary across time scales (Wang 2006; Wang et al. 2014; P. Wang et al. 2017). The recent half century has witnessed significant interdecadal changes of the East Asian summer monsoon (EASM) in the late 1970s and the early 1990s (1992–94) in terms of rainfall pattern (Ding et al. 2008, 2009; Zhou et al. 2009; Kwon et al. 2007; Yim et al. 2014). An interdecadal shift of the Indian summer monsoon (ISM) from above normal to below normal was observed around 1970 (Goswami 2006), followed by a decrease of potential predictability in the middle to late 1970s (Goswami 2004). However, the instrumental data period is too short for a robust analysis of the multidecadal variability of the monsoon.

Supplemental information related to this paper is available at the Journals Online website: https://doi.org/10.1175/JCLI-D-18-0743.s1.

Corresponding author: Jian Liu, jliu@njnu.edu.cn

DOI: 10.1175/JCLI-D-18-0743.1

Several studies have analyzed proxy monsoon records spanning the past millennium or two, most of which focus on the ISM (Zhu and Wang 2002; Sinha et al. 2011, 2015; Sankar et al. 2016; Shi et al. 2017; Goswami et al. 2015). Since the decadal to centennial variations and responses to external forcing often occur beyond regional scales, it is more proper to look at larger spatial scale rainfall reconstructions for detecting coherent changes of the EASM and ISM, as well as adjacent regions in Asia. This has not been done.

Among the major challenges to understand decadal to multidecadal climate variability are to distinguish whether such changes arise from internal coupled dynamic modes or are driven by forcings external to the coupled climate system, as well as to determine their relative contributions. In the groundbreaking work of Wang et al. (2013a), the decadal variations of the Northern Hemisphere (NH) summer monsoon rainfall are largely attributed to internal coupled dynamics even under a warming climate of twentieth century. A 500-yr preindustrial control run with a coupled Earth system model [Nanjing University of Information Science and Technology (NUIST)-ESM; Cao et al. 2015, 2018] supported the view that the multidecadal NH monsoon variations are likely results of internal variability of the Earth climate system (Wang et al. 2018). Two major sources of predictability for decadal variations of NH land monsoon rainfall are identified: a North Atlantic–southern Indian Ocean SST dipole (NAID) measured by the NAID index and an interdecadal Pacific oscillation (IPO)-like east–west Pacific Ocean SST contrast measured by the extended ENSO (XEN) index (Wang et al. 2018). It has been shown that skillful prediction of the NH land monsoon rainfall can be achieved a decade ahead by using a hybrid dynamic–empirical model (Wang et al. 2018). As an important part of the NH monsoon system, the dynamical origins of the decadal variability of the East Asian summer monsoon have also been examined. Li and Wang (2018) identified that the central-eastern tropical Pacific (CEP) cooling and the warming over the extratropical North Pacific and western tropical Pacific during May–October are linked to the decadal variation of the EASM. Numerical experiments further suggest that the CEP cooling as the major driver of the decadal East Asian land rainfall, while the western Pacific SST anomalies are largely a response (Li and Wang 2018). One may question the uncertainties associated with the model in use, or the nonstationarity associated with the empirical forecasting techniques. Now with increasing availability of long-term proxy records, we can look at these questions with reconstructed rainfall and SST indices as proxy evidences alongside the model simulation results to better address the uncertainty issue.

Building upon our previous work of the reconstructed Asian summer precipitation (RAP) (Shi et al. 2018), here we present an in-depth analysis of the decadal and multidecadal variations of the Asian summer rainfall over the past five centuries. Section 2 describes the data and methods. Section 3 presents temporal and spatial structures of the decadal and multidecadal variability. In section 4 we explore potential internal factors associated with the decadal and multidecadal variability of the Asian summer rainfall and the secular changes of these linkages. In section 5 we discuss the mechanisms associated with the decadal and multidecadal variability. Section 6 summarizes major conclusions.

2. Data and methods

a. Reconstruction, observation, and reanalysis datasets

The RAP dataset is a gridded ($2° \times 2°$) 544-yr (from AD 1470 to 2013) summer [primarily June–August (JJA)] rainfall reconstruction generated by merging two complementary proxies including 453 tree ring width chronologies and 71 historical documentary records over the Asian land region (8.75°S–55.25°N, 61.25°–143.25°E) (Shi et al. 2018). The calibration period is 1951–89, the verification period is 1901–20, and the 1921–50 period is used for weighting. Skillful reconstruction is found over East and North China, northern India and Pakistan, the Indochina Peninsula, midlatitude Asia, the Maritime Continent, and southern Japan. It has been demonstrated the RAP dataset well captures the large-scale year-to-year rainfall variability over the EASM and ISM domains (together referred to as monsoon Asia), as well as arid central Asia, and the perennial rainfall region of the Maritime Continent (MC) during the twentieth century (Shi et al. 2018). The RAP is also in general agreement with other proxies (speleothems and ice cores) during the period of 1470–1920. The remarkably abrupt change of the ISM during the 1600s recorded in the upwelling proxy over the Arabian Sea is also captured by the RAP (Shi et al. 2018).

To examine the global SST and circulation patterns associated with the decadal–multidecadal variations of the RAP over the industrial period, we have used long records of instrumental SSTs and reanalysis datasets dated back to ~1850s. One is the Kaplan Extended SST V2 (1856 to present), derived by statistically combining the monthly anomalies from the Met Office Hadley Centre historical SST dataset (MOHSST5)

of the Global Ocean Surface Temperature Atlas (GOSTA) (Kaplan et al. 1998) and the National Oceanic and Atmospheric Administration (NOAA) operational global SST analysis with in situ (ship and buoy) and satellite SST (Reynolds and Smith 1994). The other is the NOAA–Cooperative Institute for Research in Environmental Sciences (CIRES) Twentieth Century Reanalysis version 2c from 1851 to 2012 (Giese et al. 2016; Compo et al. 2006). Both datasets are provided by NOAA/OAR/ESRL PSD, Boulder, Colorado, from their website at https://www.esrl.noaa.gov/psd/. For the twentieth century, the Hadley Centre Sea Ice and Sea Surface Temperature dataset (HadISST) from 1870 to 2013 (Rayner et al. 2003) is used.

This work also utilizes a collection of climate reconstructions over the Common Era overlapping with the RAP. First, the recent reconstruction of global hydroclimate and dynamical variables (Steiger et al. 2018), which combine 2978 paleoclimate proxy data with the physical constraints from an atmosphere–ocean climate model, was used. We selected the gridded 2-m air temperature reconstruction and the reconstructed Atlantic multidecadal oscillation (AMO) index from this product. Two additional AMO indices (Mann et al. 2009; J. Wang et al. 2017) were used (see Fig. S1 in the online supplemental material). Besides, the global surface temperature field reconstructed by Mann et al. (2009) were used. Only temperature reconstructions over the Pacific Ocean are examined. It is possible that tree rings in tropical Asia and the MC used in Steiger et al. (2018) and the historical documents in South China used by Mann et al. (2009) are also included in the RAP reconstruction. But the number of the common proxies are very few (Steiger et al. 2018; Mann et al. 2009). For Steiger et al.'s (2018) reconstruction over the western Pacific, a large number of independent coral records are used in comparison with the number of tree rings after 1750 (Steiger et al. 2018). Besides, the RAP is generated by weighted combining of both tree-ring and historical-record based reconstructions. Therefore, we do not expect the correlations examined in later sections between reconstructed surface temperature over the ocean and the averaged RAP index over the entire Asian land to be significantly affected by the shared proxies.

b. *Analysis methods*

Spectral analysis and wavelet analysis were applied to detect periodicities and their long-term changes. For the spectral analysis, the forward fast Fourier transformation was used with the modified Daniell window with a span of 4 (averaging 3 periodogram estimates). Continuous wavelet transform was applied to obtain wavelet power spectrum of the normalized variance of target time series (Torrence and Compo 1998).

The empirical orthogonal function (EOF) analysis was used to display spatial features of the leading variability modes on different time scales. To separate signals of different frequencies, a 4-yr running mean minus 21-yr running mean was applied to the data (the RAP and SSTs) to extract the decadal component; a 21-yr running mean minus 45-yr running mean was applied to extract the multidecadal component. We conducted sensitivity tests by comparing the results derived from two bandpass filtering methods with 8- to 40-yr bandpass for decadal signal and 40- to 80-yr bandpass for multidecadal signal. Compared to the Lanczos bandpass/lowpass filtering (Duchon 1979), the running average method used here preserves the power/magnitude of each component better and it does not lose much data on each end of the record. The Butterworth bandpass filter (Russell 2006) could not effectively generate multidecadal signal after around 1900 compared with both the Lanczos bandpass filtering and the running average method.

Statistical tests for correlation and regression coefficients between the RAP and observed SSTs are determined by the effective degrees of freedom after taking into account the autocorrelations (Livezey and Chen 1983). A simplified Monte Carlo method following Hope (1968) is also used. It is a relatively less strict test but still enables meaningful interpretations when the correlation coefficients are relatively low.

c. *Constructing the proxy mega-ENSO index*

Mega-ENSO forcing is crucial to the decadal changes of the Asian summer rainfall (Wang et al. 2018). However, no reconstruction of such index over the past 544 years has been done in the literature. To extend the analysis beyond instrumental period, we used two gridded global surface temperature reconstructions to construct proxies representing the mega-ENSO for the period of 1470 to 2013, which is named as a proxy mega-ENSO index.

The first proxy mega-ENSO index is generated with the 2-m surface temperature reconstruction by Steiger et al. (2018), and it is well correlated with the observed yearly mega-ENSO index during 1871–2013 ($r = 0.86$, $p < 0.01$). The other one is constructed with the surface temperature field from Mann et al. (2009). It is smoother and well reflects the decadal feature of the mega-ENSO observation (4-yr smoothed mega-ENSO index) with a correlation coefficient of 0.86 ($p < 0.01$) on the decadal time scale during 1871–2013 (Fig. S1).

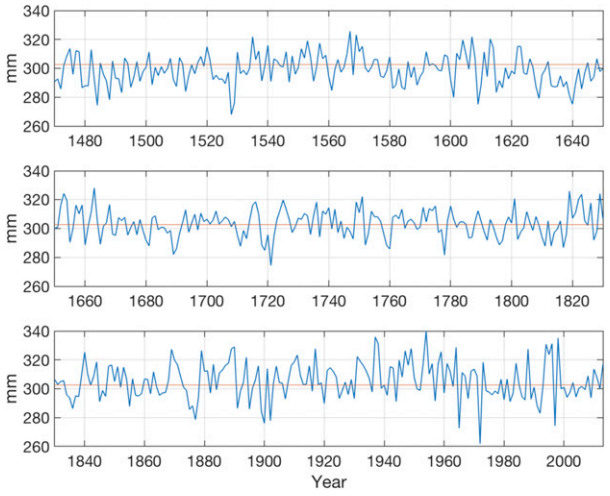

FIG. 1. Yearly all-Asian rainfall index (AARI) from 1470 to 2013. The red line is the mean rainfall (303 mm) over the entire 544 years.

To further justify the constructed proxy mega-ENSO indices, we calculated the correlation maps between the proxy mega-ENSO series and 4-yr smoothed global SSTs from 1871 to 2013 (Fig. S2). Both correlation patterns largely resemble the mega-ENSO pattern in the Pacific (Wang et al. 2013a). The AMO proxies are reconstructed by various authors and the series used are the unfiltered SST anomalies over the North Atlantic Ocean (Fig. S1).

3. Temporal–spatial structure of the decadal-multidecadal variability of RAP

a. *Major periodicities of all Asian summer rainfall (1470–2013)*

To examine the low-frequency variability of the Asian summer rainfall, we first try to identify the leading periodicities, and the periods during which they dominate. To this end, we first constructed an all-Asian summer rainfall index (AARI) by area-weighted averaging summer rainfall over the entire Asian land including the Maritime Continent. The rationale for making the AARI lies in the fact that the leading EOF mode of RAP on interannual time scale shows a nearly homogeneous spatial pattern (Shi et al. 2018). The AARI is dominated by the rainfall over monsoon Asia and the MC.

Figure 1 shows the time series of yearly AARI from 1470 to 2013. The temporal evolution involves multiple time scales, including interannual, decadal, multidecadal, and longer scales. Spectral analysis of the AARI reveals four major significant spectral peaks: interannual (2–5 yr), decadal (8–10 yr), quasi-bidecadal (22 yr), multidecadal (50–54 yr), and possibly on centennial and longer time scales (Fig. 2a). The 8–10-yr and ~50-yr periodicities had been previously found in the EOF2 and EOF3 modes of RAP in Shi et al. (2018).

In addition to the AARI, we define three regional rainfall indices basing on three major rainfall regimes over Asia, the monsoonal, the arid–semiarid, and perennial (Wang and LinHo 2002), which divide the large area of Asia south of 55°N into the monsoon Asia, arid central Asia, and MC regions. 1) The monsoon Asia domain was defined using precipitation characteristics (wet summer vs dry winter) following the criteria proposed by Wang and Ding (2008), namely that the annual range of precipitation exceeds 300 mm (or 2 mm day^{-1}) and local summer (May–September) precipitation exceeds 55% of the annual total precipitation. 2) The arid central Asia region is defined as the region north and west of the monsoon domain where the summer rainfall below 1 mm day^{-1}, and the precipitation belongs to the Mediterranean regime (dry summer vs wet winter) with the wet season occurring from December to March. 3) The MC (8.75°S–10.25°N, 95.25°–143.25°E) [Fig. 1b in Shi et al. (2018)] is a special region that includes primarily the perennial rain regime, but also a part of the MC belongs to NH and Southern Hemisphere (SH) monsoon regions in the deep tropics. Three regional boreal summer rainfall indices are calculated with area weighting.

Power spectra of the three yearly regional rainfall indices show that the 22-yr peak is found in arid Asia (Fig. 2d), while the 10- and 50-yr peaks are found in monsoon Asia (Fig. 2b) and the MC (Fig. 2c). The regional spectral analysis reveals that three subregions have collectively contributed to the major periodicities of the 544-yr AARI: the 10- and 50-yr periodicities by monsoon Asia and the MC, and the 22-yr peak by arid Asia.

b. *A sudden change of leading periodicity around 1700*

The wavelet analysis of the AARI reveals an interesting and surprising result, namely a sudden change of leading periodicity around 1700. As shown in Fig. 3, the multidecadal (~50 yr) oscillatory signal dominates the variability before 1700. However, after ~1700 the multidecadal signal nearly disappears, and meanwhile the decadal (8–22 yr) power increases. Agreeably, the variances of the AARI on decadal and multidecadal time scales show significant changes across 1700. The F test shows that the standard deviations (SD) for the two periods on both time scales are significantly different from each other at 95% significance level. The ratio between the decadal SD and multidecadal SD is 1.86 before 1700 and 3.17 after 1700. This is mainly due to the evident decrease of multidecadal variability after 1700 (Fig. 3).

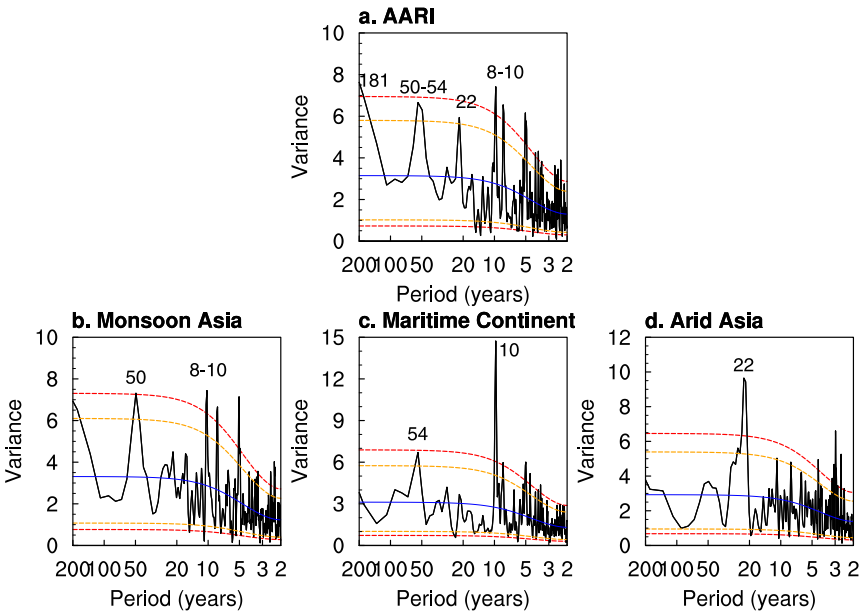

FIG. 2. Power spectra for the AARI and regional boreal summer rainfall indices. Blue curves are the Markov red noise spectra. Red and orange dashed curves indicate upper and lower confidence bounds at 95% and 90% significance levels, respectively.

To further confirm this finding, spectral analyses of the AARI and three regional indices have been applied to the two epochs, before 1700 (1470–1700) and after 1700 (1701–2013) (Fig. 4). Indeed, there exists a change of leading periodicities of the AARI around AD 1700: Before 1700, the 50-yr peak is the only significant and dominant periodicity (Fig. 4, first column top), but after 1700, the decadal and 22-yr peaks emerge and become significant periodicities (Fig. 4, first column bottom). This sudden change of leading periodicity can also be detected from all three subregional indices. As shown in Fig. 4, all three regions show significant multidecadal (50–54 yr) peaks before 1700 (Fig. 4a). After 1700, 10-yr periodicity dominates the MC, and 22-yr periodicity dominates arid Asia (Fig. 4b). Both 10- and 22-yr peaks appear in monsoon Asia.

c. *Leading mode structures of the decadal–multidecadal variability*

The leading mode of interannual variability of Asian summer rainfall shows a nearly uniform spatial pattern (Shi et al. 2018). Here we show the leading EOF modes on decadal and multidecadal time scales as well as the power spectra of the corresponding PCs (Fig. 5). Similar to the interannual variation, an overall uniform pattern is found on both the decadal and multidecadal time scales. The leading decadal mode accounts for about 24% of the total band-filtered variance with a sharp peak around 10 years. This peak is dominated by rainfall over the MC, central eastern China, Bangladesh, and India. The leading mode of multidecadal variation accounts for 31% of the total band-filtered variance with a peak around 50 years and less loading over the South Asian sector. The power spectra of the leading PCs on decadal and multidecadal time scales are consistent with the leading low-frequency periodicities of the AARI (Fig. 2a). Since the EOFs are relatively uniform, the power spectra of the PCs cannot effectively reflect information regarding regionality (Figs. 2b–d).

The two PCs are significantly ($p < 0.01$) correlated with the band-filtered AARIs on the two time scales (Fig. S3). Both the decadal and multidecadal PC1s and AARIs show slightly increased frequency after AD 1700 by eyeballing (Fig. S3), which agrees with the wavelet power spectra of the AARI (Fig. 3) and the power spectra before and after AD 1700 (Fig. 4).

4. Possible drivers of the decadal–multidecadal variability of the Asian summer rainfall

a. *SST anomalies that potentially drive the decadal variability*

In searching for the origin of the decadal variability, we first examine the global SST and circulation anomalies associated with the decadal PC1 using instrumental data

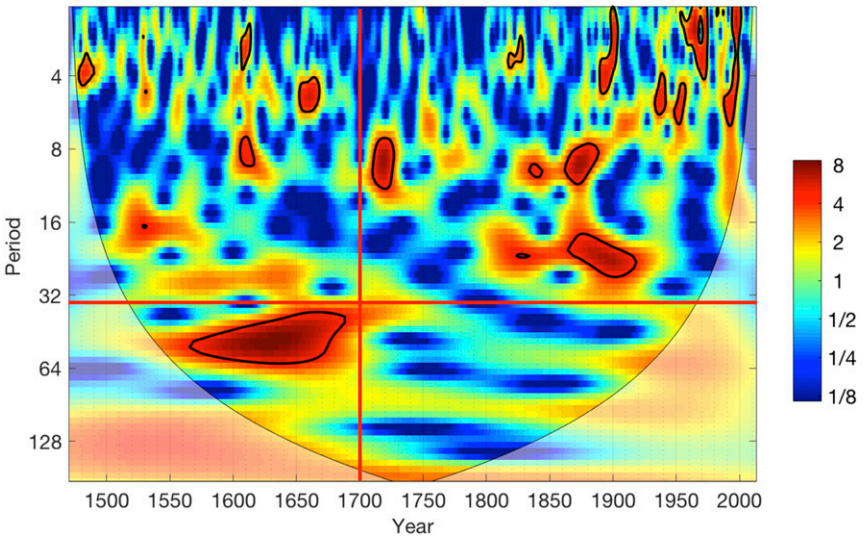

FIG. 3. Continuous wavelet power spectrum of the AARI. The black contour designates the 95% significance level against the red noise and the cone of influence (COI) where edge effects might distort the picture is shown as a lighter shade. The red vertical line marks the year 1700, and the red horizontal line divides the decadal and multidecadal periodicities.

during the industrial period (Fig. 6). The SST pattern shows an evident mega-La Niña pattern with significant warming over the western Pacific K-shaped region and cooling over the eastern Pacific triangle region (Wang et al. 2013a). Significant warming over the northern Atlantic Ocean and cooling over the southwestern Indian Ocean are also found (Fig. 6). This suggests that the leading mode of decadal variability of

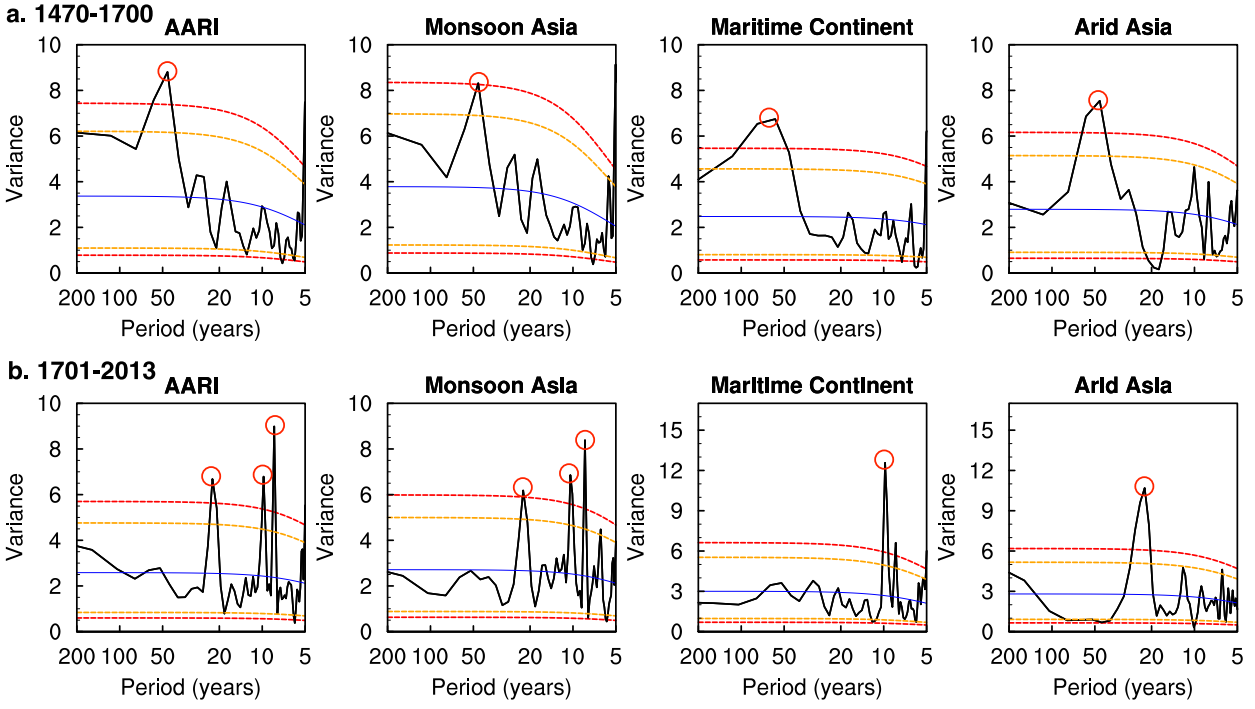

FIG. 4. Change of the dominant periodicity in Asian summer rainfall around AD 1700. The power spectra (a) before and (b) after AD 1700, respectively, for the AARI and regional boreal summer rainfall indices are shown. Blue curves are the Markov red noise spectra. Red and orange dashed curves indicate upper and lower confidence bounds at 95% and 90% significance levels, respectively.

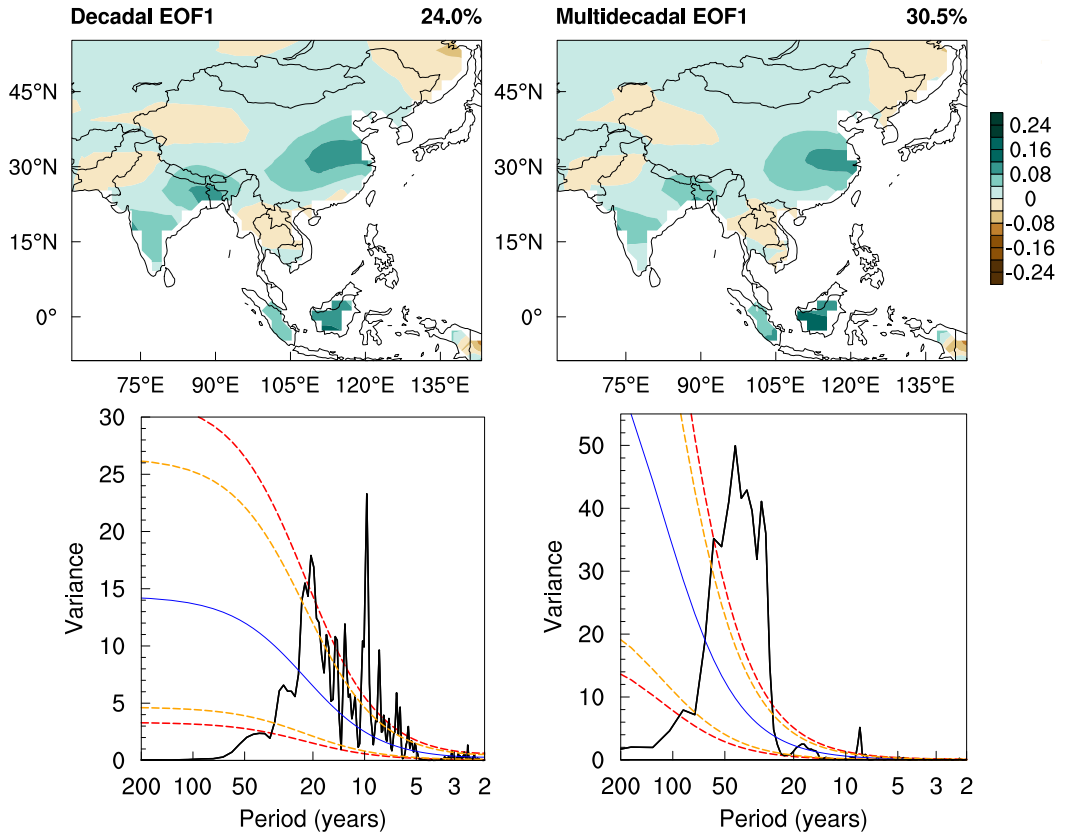

FIG. 5. Leading low-frequency modes of variability of the Asian summer rainfall for the 1470 to 2013 period. Shown are the first empirical orthogonal function (EOF) modes on decadal and multidecadal time scales, and the power spectra of corresponding principal components (PCs).

Asian summer monsoon may be rooted in the Pacific, North Atlantic, and Indian Ocean SST anomalies, particularly the mega-ENSO and AMO.

Since the instrumental data have limited length of record, we further use our reconstructed proxy mega-ENSO index and proxy AMO indices reconstructed by other authors to examine the decadal AARI variability before the instrumental period. Figure 7 shows the two proxy mega-ENSO indices constructed in section 2c and three AMO reconstructions by various authors, together with the decadal AARI for the period from 1701 to 1855. This preindustrial period is chosen because the decadal variability is more significant after 1700 (Fig. 4b). Correlation coefficients between the AARI and the mega-ENSO and AMO indices range from 0.32 to 0.39 ($p < 0.05$), indicating that the mega-ENSO and AMO are likely drivers of the decadal AARI variations during this time period. Although each only explains 10%–15% variance of the decadal variability, an agreement of significant correlations among various reconstructions indicates that these relationships are meaningful and likely widely observed.

b. *Possible internal drivers for the multidecadal variation of AAR*

For the multidecadal variation, the instrumental data period is too short to detect robust SST anomaly drivers. However, significant warming over the northern Atlantic Ocean is still found in association with the enhanced Asian summer rainfall (figure not shown), suggesting a possible linkage between the AMO and multidecadal variation of AAR. Therefore, we further examined how the multidecadal AARI is related to the same set of AMO and mega-ENSO proxy reconstructions for the period of 1470–1700 during which the multidecadal variations are prominent (Fig. 4a). As the time goes back, the two constructed proxy mega-ENSO indices deviate from each other, and only one of them shows significant positive correlation with the AARI ($r = 0.32$, $p < 0.1$) (figure not shown). On the other hand, all AMO reconstructions show stronger correlation with the multidecadal AARI (Fig. 8). The correlation coefficients range from 0.30 to 0.47 at 90% significance level or higher. This suggests that on the multidecadal time scale,

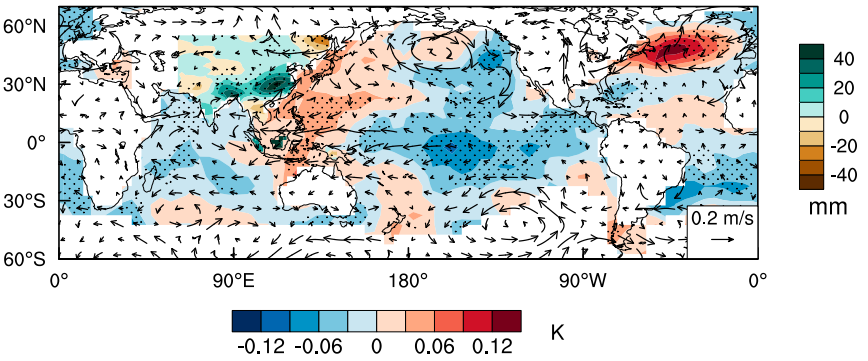

FIG. 6. Decadal summer rainfall anomalies (shading over land; horizontal color bar; unit: mm), SST anomalies (shading over the ocean; vertical color bar; unit: K), and 850-hPa winds (vectors; unit: m s^{-1}) regressed onto decadal PC1 of the reconstructed Asian summer precipitation (RAP) for the 1856 to 2013 period. The SST data are the Kaplan Extended SST V2 (Kaplan et al. 1998; Reynolds and Smith 1994). The winds are from the Twentieth Century Reanalysis version 2c (Giese et al. 2016; Compo et al. 2006). Dotted areas indicate statistically significant regression for the shadings at 95% level following Livezey and Chen (1983).

enhanced AAR is likely more associated with the warm North Atlantic.

c. *Secular changes of the decadal relationship between the AAR and mega-ENSO/AMO*

The decadal signal of the AAR is relatively strong after 1700 (Figs. 3 and 4b) and shows significant relationship with mega-ENSO and AMO (Fig. 7). Therefore, in this section, we further examine whether these relationships have changed since 1700. Rolling correlations with 101-yr window between these indices and the AARI are calculated for this purpose and the results are shown in Fig. 9. All series are 4-yr minus 21-yr running means. Considerable spread can be found among the AARI correlations

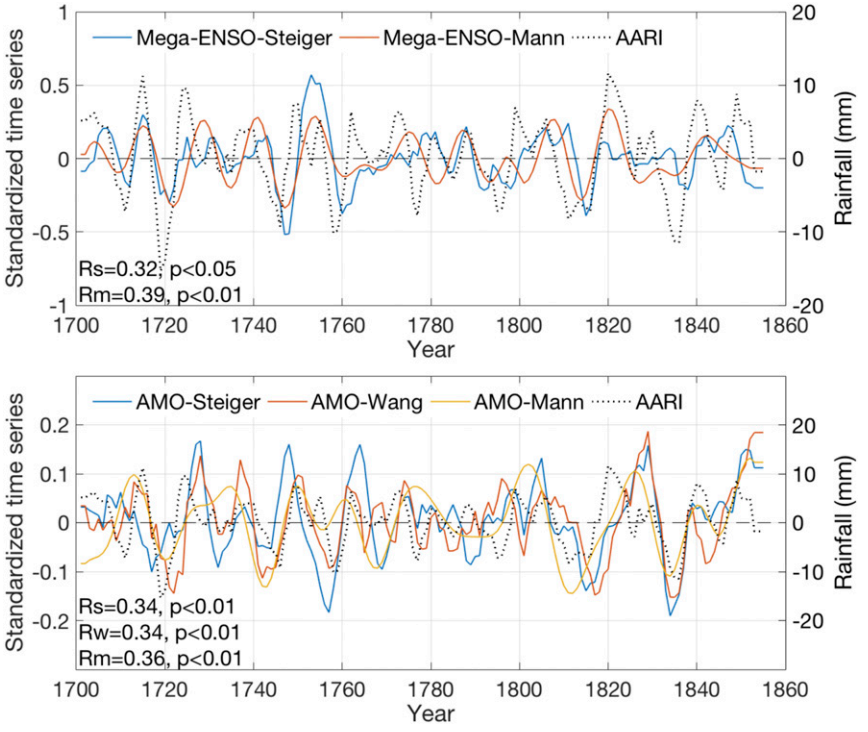

FIG. 7. Decadal AARI compared with (top) proxy mega-ENSO indices and (bottom) Atlantic multidecadal oscillation (AMO) reconstructions (bottom) for the 1701–1855 period.

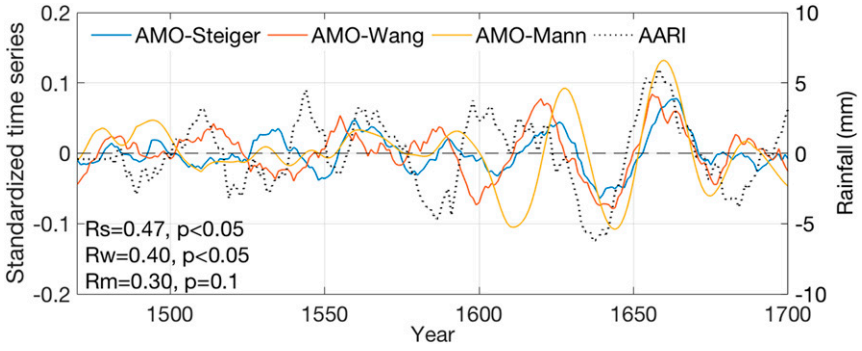

FIG. 8. Multidecadal AARI compared with the AMO reconstructions for the 1470–1700 period.

with each individual reconstructed proxy SST indices (black curves, Fig. 9), indicating that uncertainties exist with the interpretations based on their averages (thick red curves, Fig. 9).

Figure 9 shows that both relationships are nonstationary. The proxy mega-ENSO and AARI relationship is significantly positive since 1700 except for a brief weakening in the nineteenth century. However, the observations still show a significant mega-ENSO and AARI relationship after 1856 (Fig. 6). The AMO–AARI relationship, on the other hand, is significantly positive from around 1750 to 1825. After 1825, the relationship weakens and becomes negative in the late nineteenth century. Note that after 1856, the decadal AARI is associated with the extratropical North Atlantic SST anomalies (Fig. 6) rather than the SST anomalies over the entire northern Atlantic as reflected by the AMO.

Gershunov et al. (2001) proposed that the decadal modulation of the ENSO–Indian rainfall relationship could be due solely to stochastic processes. Following the bootstrapping scheme in their paper, a significance test was applied to the observed AARI relationship with the mega-ENSO and AMO in Fig. 9. The testing result indicates that the nonstationarity of the decadal AARI–AMO relationship is statistically distinguishable from what would be expected from correlated pairs of white noise time series at 95% significance level. However, for the decadal AARI and mega-ENSO relationship, we cannot rule out the possibility that the nonstationarity is caused by stochastic climate variability. Nevertheless, many studies have observed nonstationary relationships between the monsoon and internal climate modes including the AMO and PDO (Shi et al. 2017; Sankar et al. 2016; Goswami et al. 2015).

5. Mechanisms of the decadal–multidecadal variability

One driver identified for the decadal variation of the Asian summer rainfall with both observation and proxy is the mega-ENSO pattern over the Pacific Ocean (Figs. 6 and 7). Figure 6 shows that enhanced precipitation over the MC and monsoon Asia is associated with equatorial central Pacific cooling, MC and Philippine Sea warming and western Indian Ocean cooling. The SST gradients in the equatorial Pacific and Indian Ocean generate equatorial easterly anomalies in the western Pacific and westerly anomalies over the Indian Ocean, which enhances moisture convergence and monsoon rainfall over the western MC. The increased precipitation heating over the MC excites the equatorial Rossby wave response, generating a low-level cyclonic circulation anomaly extending from Sumatera to the Arabian Sea, which increases the Indian rainfall. Meanwhile, the central Pacific

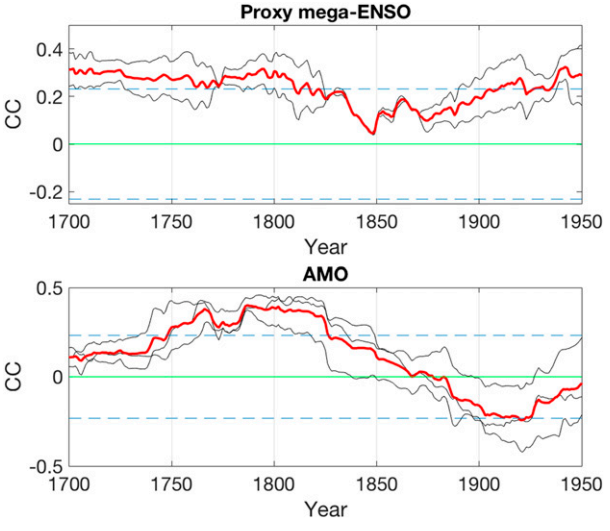

FIG. 9. Nonstationarity of decadal relationship between AARI and proxy mega-ENSO and AMO. Shown are rolling correlation coefficients with a 101-yr window. In each panel, the black curves are correlation coefficients for each individual reconstruction, and the red thick curve is averaged correlation coefficients of them. Dashed lines are cutoff correlations at the 90% significance level based on a Monte Carlo test (Hope 1968).

cooling-induced suppressed heating generates an anomalous anticyclone over the subtropical western North Pacific, which centered at the Philippine Sea with a ridge extending to Indochina peninsula. The enhanced Philippine Sea anticyclone strengthens the southwesterly monsoon, transports moist air to Bangladesh and southern China, and increases rainfall over the East China. Therefore, the decadal SST anomalies, similar to a mega-La Niña, drive atmospheric circulation and enhance Asian precipitation.

Over the Indian Ocean sector, the cooling over the southern Indian Ocean (Fig. 6) can enhance the northward temperature gradient between the Indian Ocean and the Asian continent, strengthening the Mascarene high and the cross-equatorial flow, and thus enhancing Indian monsoon rainfall (Webster et al. 1998).

Over the North Atlantic Ocean, warm anomalies occur mainly over the northern North Atlantic. The overall anomalous SST pattern over the North Atlantic resembles a warm phase of AMO or the tripolar SST anomalies associated with a negative phase of NAO. But the SST anomalies are weak except the northern North Atlantic. To what extent these SST anomalies can affect Asian precipitation is not known. Previous studies have suggested how the AMO or NAO may affect Asian precipitation in various ways. North Atlantic warming was suggested to be able to enhance Asian rainfall through a northward shift of the intertropical convergence zone (Lu et al. 2006; Zhang and Delworth 2006). Wu et al. (2009) proposed that the tripolar SST anomalies associated with a negative phase of NAO could enhance EA summer monsoon by inducing downstream development of subpolar teleconnections across the northern Eurasia, which enhances the high pressure over the Ural Mountain and the Okhotsk Sea, thereby favoring strengthened East Asian subtropical frontal rainfall. Another mechanism by which North Atlantic SST anomalies can affect EASM is through changing equatorial central Pacific SSTs. The SST anomalies associated with a negative phase of NAO in the tropical Atlantic can lead to equatorial Pacific cooling during northern summer (Gong et al. 2011; Wang et al. 2013b), which further strengthens the western Pacific subtropical high through exciting the westward propagating, descending Rossby waves, thus increasing EA rainfall. On the decadal–multidecadal time scale, a positive AMO favors more frequent negative NAO (Peings and Magnusdottir 2014) and associated tripolar SST pattern in the North Atlantic. The Atlantic SST anomalies shown in Fig. 6 can be considered as a combination of a positive AMO and negative NAO. Therefore, a positive AMO or a negative phase of NAO could have a similar or joined effect to enhance Asian precipitation. However, by analysis of the proxy records from 1701 to 1855, we found that the correlations between the RAP index and the proxy NAOs are not significant on the decadal time scale, while the correlations with the proxy AMOs are significant. This inconsistency may be due to the uncertainties in the reconstructed proxies, especially the proxy NAO indices.

6. Conclusions

Using the new reconstructed Asian summer precipitation (RAP) dataset (Shi et al. 2018) from 1470 to 2013, decadal to multidecadal variations of the Asian summer rainfall were examined. Some interesting findings are summarized as follows.

1) Significant decadal (8–10 yr), quasi-bidecadal (22 yr), and multidecadal (50–54 yr) periodicities are found in the area-averaged all-Asia rainfall index (AARI) (Figs. 1 and 2). A sudden change of the leading periodicity from multidecadal (~50 yr) to decadal and bidecadal periodicity occurred around AD 1700 (Fig. 3).
2) Further examination of three regional indices, which are area-weighted rainfall averaged over the monsoon Asia, Maritime Continent (MC), and arid Asia regions, indicates that the 10- and 50-yr peaks are from monsoon Asia and the MC, while the 22-yr peak is mainly from the arid Asia (Fig. 2); before AD 1700, the 50–54-yr peak is the only significant and dominant periodicity for all three regions, but after 1700 the decadal and 22-yr peaks become significant periodicities. Specifically, the MC is dominated by a 10-yr periodicity, arid Asia is dominated by a 22-yr periodicity, and monsoon Asia exhibits both 10- and 20-yr periodicities (Fig. 4).
3) The leading EOF modes on the decadal and multidecadal time scales both exhibit a similar spatially uniform structure, suggesting a nearly in-phase variations among the rainfall over South Asia and East Asia, as well as the MC on decadal and multidecadal time scales (Fig. 5). The leading PCs are significantly correlated with the AARI on each time scale (Fig. S3).
4) The leading decadal mode of reconstructed Asian summer rainfall variability is associated with a mega-ENSO pattern (Figs. 6 and 7). The AARI–mega-ENSO relationship is persistently significant except from 1820 to around 1900 (Fig. 9). Long SST and reanalysis data as well as paleoclimate reconstructions indicate that the enhanced decadal AAR is also significantly associated with North Atlantic warming/positive AMO (Figs. 6 and 7). The AARI–AMO relationship, however, is notably nonstationary (Fig. 9).

5) Multidecadal variation (50–54 yr) of the AARI is significantly correlated with the AMO (Fig. 8). The period of strong correlation between the AMO and the multidecadal AARI coincides with the strong ~50-yr periodicity of the AARI (Fig. 3).

The present study shows evidence that decadal–multidecadal variations of the Asian monsoon are associated with internal coupled dynamic modes. However, with observation and paleoclimate reconstructions only, we cannot fully distinguish whether these "internal" signals are truly internal or a mixture of natural and forced responses. Especially, the study period covers the coldest part of the Little Ice Age (LIA) and current unprecedented warming featuring many changes in the climate system associated with the transition between the two eras (e.g., changes in solar radiative forcing, volcanic activities, and greenhouse gas concentration). These changes in external forcing may alter certain properties of the internal modes, or create SST anomalies that resemble the internal mode variability, which further influence the global circulation/rainfall. Future work with forced/unforced runs and model experiments can help to test this hypothesis.

Acknowledgments. We appreciate the comments from the editor and reviewers, which led to the improved manuscript. This work is supported by the National Natural Science Foundation of China (Grant 41420104002), the National Key Research and Development Program of China (Grant 2016YFA0600401), and the National Science Foundation (Climate Dynamics Division) Award AGS-1540783. This is publication No. 10763 of the SOEST, publication No. 1398 of IPRC, and publication No. 276 of Earth System Modeling Center (ESMC). Support for the Twentieth Century Reanalysis Project version 2c dataset is provided by the U.S. Department of Energy, Office of Science Biological and Environmental Research (BER), and by the National Oceanic and Atmospheric Administration Climate Program Office.

REFERENCES

Cao, J., B. Wang, B. Xiang, J. Li, T. Wu, X. Fu, L. Wu, and J. Min, 2015: Major modes of short-term climate variability in the newly developed NUIST Earth System Model (NESM). *Adv. Atmos. Sci.*, **32**, 585–600, https://doi.org/10.1007/s00376-014-4200-6.

——, and Coauthors, 2018: The NUIST Earth System Model (NESM) version 3: Description and preliminary evaluation. *Geosci. Model Dev.*, **11**, 2975–2993, https://doi.org/10.5194/gmd-11-2975-2018.

Compo, G. P., J. S. Whitaker, and P. D. Sardeshmukh, 2006: Feasibility of a 100-year reanalysis using only surface pressure data. *Bull. Amer. Meteor. Soc.*, **87**, 175–190, https://doi.org/10.1175/BAMS-87-2-175.

Ding, Y., Z. Wang, and Y. Sun, 2008: Inter-decadal variation of the summer precipitation in East China and its association with decreasing Asian summer monsoon. Part I: Observed evidences. *Int. J. Climatol.*, **28**, 1139–1161, https://doi.org/10.1002/joc.1615.

——, Y. Sun, Z. Wang, Y. Zhu, and Y. Song, 2009: Inter-decadal variation of the summer precipitation in China and its association with decreasing Asian summer monsoon Part II: Possible causes. *Int. J. Climatol.*, **29**, 1926–1944, https://doi.org/10.1002/joc.1759.

Duchon, C. E., 1979: Lanczos filtering in one and two dimensions. *J. Appl. Meteor.*, **18**, 1016–1022, https://doi.org/10.1175/1520-0450(1979)018<1016:LFIOAT>2.0.CO;2.

Gershunov, A., N. Schneider, and T. Barnett, 2001: Low-frequency modulation of the ENSO–Indian monsoon rainfall relationship: Signal or noise? *J. Climate*, **14**, 2486–2492, https://doi.org/10.1175/1520-0442(2001)014<2486:LFMOTE>2.0.CO;2.

Giese, B. S., H. F. Seidel, G. P. Compo, and P. D. Sardeshmukh, 2016: An ensemble of ocean reanalyses for 1815–2013 with sparse observational input. *J. Geophys. Res. Oceans*, **121**, 6891–6910, https://doi.org/10.1002/2016JC012079.

Gong, D.-Y., J. Yang, S.-J. Kim, Y. Gao, D. Guo, T. Zhou, and M. Hu, 2011: Spring Arctic Oscillation–East Asian summer monsoon connection through circulation changes over the western North Pacific. *Climate Dyn.*, **37**, 2199–2216, https://doi.org/10.1007/S00382-011-1041-1.

Goswami, B. N., 2004: Interdecadal change in potential predictability of the Indian summer monsoon. *Geophys. Res. Lett.*, **31**, L16208, https://doi.org/10.1029/2004GL020337.

——, 2006: The Asian monsoon: Inter-decadal variability. *The Asian Monsoon*, B. Wang, Ed., Springer, 295–328.

——, R. H. Kripalani, H. P. Borgaonkar, and B. Preethi, 2015: Multi-decadal variability in Indian summer monsoon rainfall using proxy data. *Climate Change: Multidecadal and Beyond*, C.-P. Chang et al., Eds., World Scientific Series on Asia-Pacific Weather and Climate, Vol. 6, 327–345.

Hope, A. C. A., 1968: A simplified Monte Carlo significance test procedure. *J. Roy. Stat. Soc.*, **30B**, 582–598, https://doi.org/10.1111/j.2517-6161.1968.TB00759.X.

Kaplan, A., M. A. Cane, Y. Kushnir, A. C. Clement, M. B. Blumenthal, and B. Rajagopalan, 1998: Analyses of global sea surface temperature 1856–1991. *J. Geophys. Res.*, **103**, 18 567–18 589, https://doi.org/10.1029/97JC01736.

Kwon, M. H., J. G. Jhun, and K. J. Ha, 2007: Decadal change in East Asian summer monsoon circulation in the mid-1990s. *Geophys. Res. Lett.*, **34**, L21706, https://doi.org/10.1029/2007GL031977.

Li, J., and B. Wang, 2018: Origins of the decadal predictability of East Asian land summer monsoon rainfall. *J. Climate*, **31**, 6229–6243, https://doi.org/10.1175/JCLI-D-17-0790.1.

Livezey, R. E., and W. Y. Chen, 1983: Statistical field significance and its determination by Monte Carlo techniques. *Mon. Wea. Rev.*, **111**, 46–59, https://doi.org/10.1175/1520-0493(1983)111<0046:SFSAID>2.0.CO;2.

Lu, R., B. Dong, and H. Ding, 2006: Impact of the Atlantic multidecadal oscillation on the Asian summer monsoon. *Geophys. Res. Lett.*, **33**, L24701, https://doi.org/10.1029/2006GL027655.

Mann, M. E., and Coauthors, 2009: Global signatures and dynamical origins of the little ice age and medieval climate anomaly. *Science*, **326**, 1256–1260, https://doi.org/10.1126/science.1177303.

Peings, Y., and G. Magnusdottir, 2014: Forcing of the wintertime atmospheric circulation by the multidecadal fluctuations of the North Atlantic Ocean. *Environ. Res. Lett.*, **9**, 034018, https://doi.org/10.1088/1748-9326/9/3/034018.

Rayner, N. A., D. E. Parker, E. B. Horton, C. K. Folland, L. V. Alexander, D. P. Rowell, E. C. Kent, and A. Kaplan, 2003: Global analyses of sea surface temperature, sea ice, and night marine air temperature since the late nineteenth century. *J. Geophys. Res.*, **108**, 4407, https://doi.org/10.1029/2002JD002670.

Reynolds, R. W., and T. M. Smith, 1994: Improved global sea surface temperature analyses using optimum interpolation. *J. Climate*, **7**, 929–948, https://doi.org/10.1175/1520-0442(1994)007<0929:IGSSTA>2.0.CO;2.

Russell, D., 2006: Electronic supplement to "Development of a time-domain, variable-period surface wave magnitude procedure for application at regional and teleseismic distances, Part I: Theory." *Bull. Seismol. Soc. Amer.*, **96**, 665–677, http://www.seismosoc.org/Publications/BSSA_html/bssa_96-2/05055-esupp/.

Sankar, S., L. Svendsen, B. Gokulapalan, P. V. Joseph, and O. M. Johannessen, 2016: The relationship between Indian summer monsoon rainfall and Atlantic multidecadal variability over the last 500 years. *Tellus*, **68A**, 31717, https://doi.org/10.3402/tellusa.v68.31717.

Shi, F., K. Fang, C. Xu, Z. Guo, and H. P. Borgaonkar, 2017: Interannual to centennial variability of the South Asian summer monsoon over the past millennium. *Climate Dyn.*, **49**, 2803–2814, https://doi.org/10.1007/s00382-016-3493-9.

Shi, H., B. Wang, E. R. Cook, J. Liu, and F. Liu, 2018: Asian summer precipitation over the past 544 years reconstructed by merging tree rings and historical documentary records. *J. Climate*, **31**, 7845–7861, https://doi.org/10.1175/JCLI-D-18-0003.1.

Sinha, A., M. Berkelhammer, L. Stott, M. Mudelsee, H. Cheng, and J. Biswas, 2011: The leading mode of Indian summer monsoon precipitation variability during the last millennium. *Geophys. Res. Lett.*, **38**, L15703, https://doi.org/10.1029/2011GL047713.

——, G. Kathayat, H. Cheng, S. F. M. Breitenbach, M. Berkelhammer, M. Mudelsee, J. Biswas, and R. L. Edwards, 2015: Trends and oscillations in the Indian summer monsoon rainfall over the last two millennia. *Nat. Commun.*, **6**, 6309, https://doi.org/10.1038/ncomms7309.

Steiger, N. J., J. E. Smerdon, E. R. Cook, and B. I. Cook, 2018: A reconstruction of global hydroclimate and dynamical variables over the Common Era. *Sci. Data*, **5**, 180086, https://doi.org/10.1038/sdata.2018.86.

Torrence, C., and G. P. Compo, 1998: A practical guide to wavelet analysis. *Bull. Amer. Meteor. Soc.*, **79**, 61–78, https://doi.org/10.1175/1520-0477(1998)079<0061:APGTWA>2.0.CO;2.

Wang, B., 2006: *The Asian Monsoon*. Springer, 787 pp.

——, and LinHo, 2002: Rainy season of the Asian-Pacific summer monsoon. *J. Climate*, **15**, 386–398, https://doi.org/10.1175/1520-0442(2002)015<0386:RSOTAP>2.0.CO;2.

——, and Q. Ding, 2008: Global monsoon: Dominant mode of annual variation in the tropics. *Dyn. Atmos. Oceans*, **44**, 165–183, https://doi.org/10.1016/j.dynatmoce.2007.05.002.

——, J. Liu, H.-J. Kim, P. J. Webster, S.-Y. Yim, and B. Xiang, 2013a: Northern Hemisphere summer monsoon intensified by mega-El Niño/Southern Oscillation and Atlantic multidecadal oscillation. *Proc. Natl. Acad. Sci. USA*, **110**, 5347–5352, https://doi.org/10.1073/pnas.1219405110.

——, B. Xiang, and J.-Y. Lee, 2013b: Subtropical high predictability establishes a promising way for monsoon and tropical storm predictions. *Proc. Natl. Acad. Sci. USA*, **110**, 2718–2722, https://doi.org/10.1073/pnas.1214626110.

——, and Coauthors, 2018: Toward predicting changes in the land monsoon rainfall a decade in advance. *J. Climate*, **31**, 2699–2714, https://doi.org/10.1175/JCLI-D-17-0521.1.

Wang, J., B. Yang, F. C. Ljungqvist, J. Luterbacher, T. J. Osborn, K. R. Briffa, and E. Zorita, 2017: Internal and external forcing of multidecadal Atlantic climate variability over the past 1,200 years. *Nat. Geosci.*, **10**, 512–517, https://doi.org/10.1038/ngeo2962.

Wang, P. X., B. Wang, H. Cheng, J. Fasullo, Z. T. Guo, T. Kiefer, and Z. Y. Liu, 2014: The global monsoon across timescales: Coherent variability of regional monsoons. *Climate Past*, **10**, 2007–2052, https://doi.org/10.5194/cp-10-2007-2014.

——, ——, ——, ——, Z. Guo, T. Kiefer, and Z. Liu, 2017: The global monsoon across time scales: Mechanisms and outstanding issues. *Earth Sci. Rev.*, **174**, 84–121, https://doi.org/10.1016/j.earscirev.2017.07.006.

Webster, P. J., V. O. Magaña, T. N. Palmer, J. Shukla, R. A. Tomas, M. Yanai, and T. Yasunari, 1998: Monsoons: Processes, predictability, and the prospects for prediction. *J. Geophys. Res. Oceans*, **103**, 14 451–14 510, https://doi.org/10.1029/97JC02719.

Wu, Z., B. Wang, J. Li, and F. F. Jin, 2009: An empirical seasonal prediction model of the East Asian summer monsoon using ENSO and NAO. *J. Geophys. Res.*, **114**, D18120, https://doi.org/10.1029/2009JD011733.

Yim, S. Y., B. Wang, and M. H. Kwon, 2014: Interdecadal change of the controlling mechanisms for East Asian early summer rainfall variation around the mid-1990s. *Climate Dyn.*, **42**, 1325–1333, https://doi.org/10.1007/s00382-013-1760-6.

Zhang, R., and T. L. Delworth, 2006: Impact of Atlantic multidecadal oscillations on India/Sahel rainfall and Atlantic hurricanes. *Geophys. Res. Lett.*, **33**, L17712, https://doi.org/10.1029/2006GL026267.

Zhou, T., D. Gong, J. Li, and B. Li, 2009: Detecting and understanding the multi-decadal variability of the East Asian summer monsoon—Recent progress and state of affairs. *Meteor. Z.*, **18**, 455–467, https://doi.org/10.1127/0941-2948/2009/0396.

Zhu, J., and S. Wang, 2002: 80 yr oscillation of summer rainfall over North China and East Asian summer monsoon. *Geophys. Res. Lett.*, **29**, 1672, https://doi.org/10.1029/2001GL013997.